JACS
JOURNAL OF THE AMERICAN CHEMICAL SOCIETY

Article

pubs.acs.org/JACS

Conformational Basis for Asymmetric Seeding Barrier in Filaments of Three- and Four-Repeat Tau

Ayisha Siddiqua,[†] Yin Luo,[‡] Virginia Meyer,[†] Michael A. Swanson,[†] Xiang Yu,[§] Guanghong Wei,[‡] Jie Zheng,[§] Gareth R. Eaton,[†] Buyong Ma,[∥] Ruth Nussinov,[∥,⊥] Sandra S. Eaton,[†] and Martin Margittai*[,†]

[†]Department of Chemistry and Biochemistry, University of Denver, Denver, Colorado 80208, United States

[‡]State Key Laboratory of Surface Physics, Key Laboratory for Computational Physical Sciences (MOE), and Department of Physics, Fudan University, Shanghai, P.R. China

[§]Department of Chemical & Biomolecular Engineering, The University of Akron, Akron, Ohio 44325, United States

[∥]Basic Research Program, SAIC-Frederick, Inc., Center for Cancer Research Nanobiology Program, Frederick National Laboratory for Cancer Research, National Cancer Institute, Frederick, Maryland 21702, United States

[⊥]Sackler Institute of Molecular Medicine, Department of Human Genetics and Molecular Medicine Sackler School of Medicine, Tel Aviv University, Tel Aviv 69978, Israel

Supporting Information

ABSTRACT: Tau pathology in Alzheimer's disease is intimately linked to the deposition of proteinacious filaments, which akin to infectious prions, have been proposed to spread via seeded conversion. Here we use double electron−electron resonance (DEER) spectroscopy in combination with extensive computational analysis to show that filaments of three- (3R) and four-repeat (4R) tau are conformationally distinct. Distance measurements between spin labels in the third repeat, reveal tau amyloid filaments as ensembles of known β-strand−turn−β-strand U-turn motifs. Whereas filaments seeded with 3R tau are structurally homogeneous, filaments seeded with 4R tau are heterogeneous, composed of at least three distinct conformers. These findings establish a molecular basis for the seeding barrier between different tau isoforms and offer a new powerful approach for investigating the composition and dynamics of amyloid fibril ensembles.

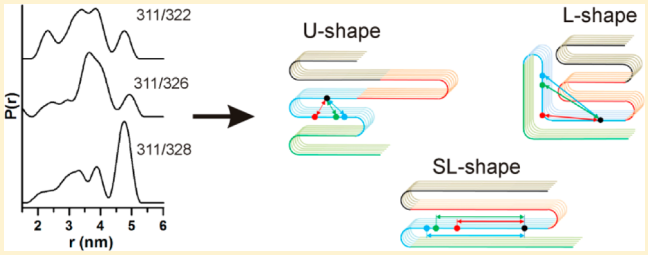

INTRODUCTION

Tau filaments are the pathological hallmark of numerous neurodegenerative diseases, including Alzheimer's disease, Pick's disease, and progressive supranuclear palsy.[1,2] Six different tau isoforms are expressed in the adult human brain, which have zero, one, or two inserts in the N-terminus and three or four semiconserved microtubule binding repeats in the C-terminus. Based on the latter repeats, half of the isoforms are classified as three-repeat (3R) tau and the other half as four-repeat (4R) tau.[3] In Alzheimer's disease, all isoforms are deposited into filaments.[4] In Pick's disease and progressive supranuclear palsy, only the 3R and 4R tau isoforms are deposited, respectively.[5] The reasons for these differences in deposition are unknown.

Upon aggregation of intrinsically disordered tau, the repeat region becomes protease resistant,[6] while the flanking regions remain in a fuzzy disordered state.[7] In vitro, filament formation is induced by the addition of negatively charged cofactors, such as heparin.[8] Removal of the flanking regions produces truncated forms of tau that contain only the repeat region: K18 for 4R tau and K19 for 3R tau.[9] The truncated proteins show greatly accelerated aggregation kinetics.[9] The formation of tau filaments is a nucleated process with an initial lag phase that is eliminated by the addition of filament seeds.[10] This aggregation property is very similar to that of other amyloid fibrils.[11] On the structural level, filaments of truncated[12] and full length[13] tau are characterized by highly ordered conformations in which β-strands run perpendicular to the long fiber axis. This strand arrangement is a common feature of all amyloid fibrils,[14] including those of prion proteins.[15] However, core sizes and β-sheet interactions can vary substantially. Even proteins with the same amino acid sequence can populate fibrils with different conformations.[16,17] In the case of prion proteins, it is thought that this structural polymorphism is a major contributor to phenotypic diversity.[18] Although tauopathies are not transmissible between organisms, new evidence indicates that tau filaments can be transferred between cells[19,20] and spread throughout the brain.[21] In this process, tau is recruited into the filament resulting in the conversion of normal tau into the misfolded state.[22] A variable U-turn-based structural core of tau filaments has been proposed to promote cross-talk with the amyloid-β peptide, suggesting that nonhomologous proteins can interact given the right

Received: April 11, 2012
Published: June 4, 2012

   dx.doi.org/10.1021/ja303498q | J. Am. Chem. Soc. 2012, 134, 10271−10278

structural context.[23,24] Interestingly, different isoforms of tau are characterized by an asymmetric seeding barrier, in which filaments of 3R tau can recruit 4R tau; however, filaments of 4R tau cannot recruit 3R tau.[25] As the seeding barrier could explain the preferential deposition of 4R tau in progressive supranuclear palsy and other 4R tauopathies, it is important to understand the molecular basis for this barrier. We used double electron−electron resonance (DEER) spectroscopy[26,27] in combination with molecular modeling as a new approach to determine conformational differences between 3R and 4R tau filaments. We anticipate that a similar strategy could reveal structural differences between fibrils in other amyloid systems and aid in the understanding of species spreading and interneuronal transmission of "infectious" conformational diseases.

EXPERIMENTAL PROCEDURES

Mutagenesis. The single cysteine mutant K311C of K18 and K19, cloned into pET-28b,[3] served as template for the generation of the double cysteine mutants K311C/C322C, K311C/G326C, and K311C/I328C. Mutagenesis was performed using the QuikChange method from Stratagene/Agilent Technologies. The correctness of all sequences was verified by DNA sequencing.

Protein Expression and Purification. Protein expression and purification were performed as previously described.[3] In short, after isopropyl-β-D-thiogalactopyranoside (IPTG)-induced overexpression, *Escherichia coli*, strain BL21 (DE3), was pelleted and taken up in resuspension buffer (20 mM piperazine-*N*,*N*′-bis(2-ethanesulfonic acid) (PIPES), pH 6.5, 500 mM NaCl, 1 mM ethylenediaminetetraacetic acid (EDTA), 50 mM β-mercaptoethanol). The cells were heated to 80 °C for 20 min and then sonicated on ice. The samples were centrifuged at 15 000 × g for 30 min. Heat stable tau protein was precipitated from the supernatant by addition of ammonium sulfate (55−60% m/V). After 1 h incubation at 25 °C, the sample was centrifuged for 10 min at 15 000 × g. The protein pellet was resuspended in H_2O (2 mM dithienothiophene (DTT)), and the solution was sonicated for 30 s, syringe filtered, and loaded onto a cation exchange column (Mono S, GE Healthcare). Proteins were eluted with a linear NaCl gradient (50−1000 mM NaCl, 10 mM PIPES, pH 6.5, 2 mM DTT). Protein fractions were analyzed by sodium dodecyl sulfate polyacrylamide gel electrophoresis (SDS-PAGE), and appropriate fractions were pooled and stored at −80 °C. Samples were further purified by gel filtration (Superdex 200 column, GE Healthcare) using a Tris buffer for elution (20 mM Tris, pH 7.4, 100 mM NaCl, 1 mM EDTA, 1 mM DTT). Pooled protein fractions were precipitated overnight at 4 °C by addition of a three-fold volumetric excess of acetone (5 mM DTT). The proteins were centrifuged (15 000 × g for 10 min), redistributed into equal aliquots, and washed with acetone (2 mM DTT). All pellets were stored at −80 °C until further use.

Protein Preparation and Labeling. Protein pellets of double cysteine mutants were solubilized in 200 μL of 8 M guanidine hydrochloride. An approximately 10-fold molar excess of paramagnetic label [1-oxyl-2,2,5,5-tetramethyl-Δ3-pyrroline-3-methyl]-methanethiosulfonate (Toronto Research Chemicals, Downsview, Toronto) was added. Samples were incubated for 1 h at 25 °C. Proteins were then passed over PD-10 desalting columns (GE Healthcare) to remove denaturant and excess label. The elution buffer consisted of 100 mM NaCl, 10 mM HEPES, pH 7.4, and 1 mM NaN_3. Samples of wild-type tau (K18 and K19 with cysteines replaced by serines) were processed the same way as double cysteine mutants with the exception that no label was added. Protein concentrations were determined by the bicinchoninic acid (BCA) method (Pierce).

Multistep Seed Production. For initial filament formation, 25 μM of wild-type tau (in elution buffer) was combined with a two-fold molar excess of heparin (average molecular mass of 5000 Da, Celsus, Cincinnati, OH) and incubated for three days at 25 °C under agitation. Seeds were produced by sonicating the samples for 20 s on ice at power setting 3 using a Fisher Scientific sonifier (150 T Series) equipped with a 3 mm tip. To 25 μM wild type tau and 50 μM heparin, 10% seeds (based on monomer concentration) were added. Fibril growth proceeded for 1 h at 37 °C.

Again, seeds were produced, and the formation of the next set of filaments initiated. The procedure was performed a total of four times. Seeds from the last cycle were used for DEER sample preparation. It was assumed that multiple steps of seeding and growth would result in homogeneous filaments. Interestingly though, polymorphic filaments were observed even after multiple cycles of seeding (see Results Section).

Sample Preparation for DEER Experiments. Filaments for DEER measurements were prepared by mixing doubly spin labeled tau mutants of K18 or K19 with a 50-fold molar excess of the corresponding wild-type constructs (total protein concentration = 50 μM), 5% seeds from the fourth seeding cycle (above), and heparin (protein:heparin molar ratio of 4:1). After 14 h incubation at 37 °C, the filaments were pelleted at 100 000 × g and washed once with elution buffer. The final filament pellets were taken up in 20−50 μL elution buffer, transferred into quartz capillaries (1.1 mm inner diameter × 1.6 mm outer diameter) and centrifuged for 20 min at 1000 × g. Residual buffer layered over the filaments was removed with a syringe. To test for short-range spin−spin interactions, continuous wave electron paramagnetic resonance (CW EPR) spectra were taken at 25 °C (see Supporting Information). Subsequently, capillary tubes were flash frozen in liquid N_2 and stored at −80 °C until further measurement.

DEER Data Acquisition and Analysis. DEER data were obtained at Q-band frequencies (34 GHz) with a Bruker Elexsys E580 spectrometer equipped with a 1 W amplifier, a Bruker ER 5107 Q-band dielectric pulse resonator, and an Oxford CF 935 cryostat. Measurements were performed using four-pulse DEER experiment: $\pi/2(\nu_{obs}) - \tau_1 - \pi(\nu_{obs}) - t' - \pi(\nu_{pump}) - (\tau_1 + \tau_2 - t') - \pi(\nu_{obs}) - \tau_2 -$ echo.[27] The resonator was fully overcoupled ($Q \sim 100$). All measurements were performed at a temperature of 80 K. The observer pulse lengths $\pi/2$ and π were optimized for each measurement and ranged from 30−40 and 60−80 ns, respectively. A pump pulse length of 40 ns was used, and τ_1 and τ_2 were kept constant, while time t' was varied. Data analysis was performed for dipolar evolution times $t = t' - \tau_1 > 0$. The pump frequency, ν_{pump}, was set to the center of the resonator dip, and the magnetic field was set in the center of the nitroxide EPR spectrum. The observe frequency, $\nu_{observer}$, was 37 MHz higher than ν_{pump}, which is a 13 G offset to lower field.[28] The shot repetition time was calculated for each run as 1.2 times the T_1 relaxation time,[29] usually between 500 and 550 μs, and eight-step phase cycling was used. The total measurement time for each sample was 48−72 h. T_1 values were obtained from inversion recovery curves by fitting with a single exponential to obtain an average value for the heterogeneous filaments. These values were not significantly different between constructs or mutants and were comparable to values obtained by fitting with multiexponential functions. Results were the same for data collected with longer shot repetition times.

DEER data were analyzed using "DeerAnalysis2011",[30] a program that can extract distance distributions from dead-time free pulse electron−electron double resonance (ELDOR) data (constant-time and variable-time pulse DEER). A background correction is first performed to ensure that intermolecular distances are suppressed. Only intramolecular distances are taken into account when calculating the distance distribution in the protein. The background correction was done using a 3D homogeneous function, and the data were fit using Tikhonov regularization with a regularization parameter, α, of 100.

Computational Simulation and Analysis. Molecular dynamics simulations were performed by the NAMD program[31] using the Charmm27 force field. The tau oligomers were energy minimized and explicitly solvated in a TIP3P water box with a minimum distance of 15 Å from any edge of the box to any tau atom. Counterions of NaCl were added to neutralize the systems. Both equilibrium and production runs were performed using an NPT ensemble under periodic boundary condition. Constant pressure (1 atm) and

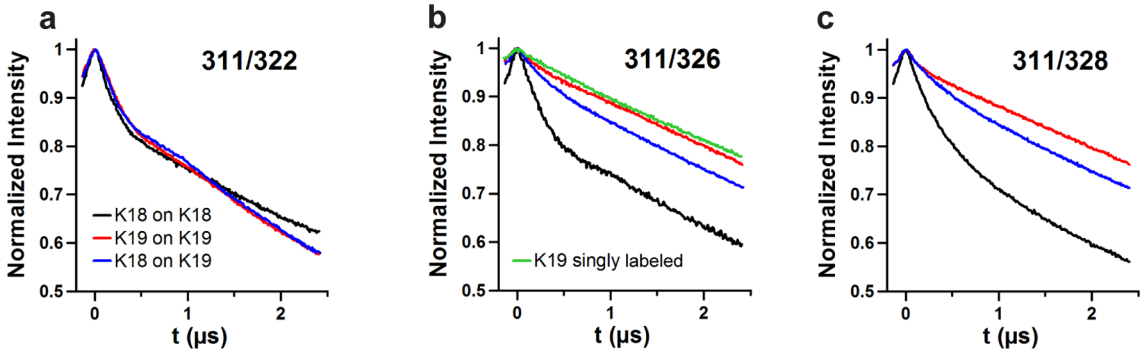

Figure 1. Dipolar oscillation traces reveal major structural differences between K18 and K19 filaments. Filaments were grown through seeded reactions with monomeric tau labeled at positions 311/322 (a), 311/326 (b), and 311/328 (c): K18 grown on K18 seeds (black traces), K19 grown on K19 seeds (red traces), and K18 grown on K19 seeds (blue traces). The green trace in the center panel is from singly labeled K19 monomers (311 and 326) grown onto K19 seeds. The dipolar traces for positions 311/326 and 311/328 indicate different spin interactions and hence different structures for K18- versus K19-seeded filaments. Labeled protein: 1 μM, unlabeled protein: 50 μM, seeds: 5% (mol:mol).

temperature (310 K) were maintained by an isotropic Langevin barostat with a decay period of 100 fs and a Langevin thermostat with a damping coefficient of 5 ps^{-1}. The long-range electrostatic interactions were treated by the particle mesh Ewald (PME) method using a real space cutoff of 12 Å and a grid size of ~1 Å in all directions. The short-range van der Waals (vdW) interactions were calculated using a switching function with a twin range cutoff of 10 and 12 Å. The velocity Verlet integrator with a time step of 2 fs was used to solve Newton's equation of motion. In the MD-MC rotamer simulations, we labeled two dihedrals: N−Cα−Cβ−Sγ for the first mutated residue (χ1) and the second mutated residue (χ2). Both χ1 and χ2 were rotated from 0 to 360° by 6° interval, resulting in the 60 × 60 rotamer combinations. Each of the 3600 (χ1, χ2) pair rotamers was subjected to 3000 step energy minimization and 2000 step molecular dynamics to obtain the fully relaxed structure. The probability distributions of nitroxide distance in the 3600 rotamers were calculated based on the Boltzmann energy distributions, using an in-house MC algorithm.[32]

RESULTS

Templated Growth Produces a New Type of 4R Tau Filaments. DEER spectroscopy allows the determination of distances between pairs of paramagnetic labels that are separated by 2−5 nm.[27,29] Recent DEER experiments have provided structural information on single amyloid fibril conformers of islet amyloid polypeptide[33] and α-synuclein.[34] Here, we set out to test whether this approach is able to distinguish between filament conformers of 3R and 4R tau. As a first step, we generated the double cysteine mutants 311/322, 311/326, and 311/328 of K18 and K19. All mutations were located in the R3, which forms a stable core with parallel, in-register arrangement of β-strands in the filament.[3,35] All mutants were labeled with the thiol-reactive nitroxide label [1-oxyl-2,2,5,5-tetramethyl-Δ3-pyrroline-3-methyl] methanethiosulfonate. Filament formation was induced by the addition of heparin (tau:heparin ratio of 4:1 (n:n)). CW EPR analysis of these samples at room temperature revealed single-line spectra (Figure S1, Supporting Information), characteristic of spin exchange between stacked labels along the long fiber axis.[36] Importantly, these experiments demonstrate that double labeling of tau in this region does not perturb the filament core but retains the parallel, in-register arrangement of β-strands.

To measure the interspin distances between the two labels within individual tau molecules, intermolecular spin−spin interactions along the fiber axis had to be minimized. For this purpose all labeled proteins were mixed with their respective "wild-type" counterparts at a 1:50 molar ratio. Specifically, doubly labeled K18 was mixed with cysteine-free K18, and doubly labeled K19 was mixed with cysteine-free K19. These monomer mixtures were grown onto the seeds produced from cysteine-free K18 or K19 filaments (see Experimental Procedures Section). We investigated three different seeding schemes: (1) K18 grown on K18 seeds, (2) K19 grown on K19 seeds, and (3) K18 grown on K19 seeds. The monomers successfully grew onto the templates in all cases. The filamentous nature of the aggregates was verified by negative stain electron microscopy (Figure S2, Supporting Information). CW EPR measurements of the sedimented filaments revealed no spectral broadening for any of the spin pairs (Figure S3, Supporting Information), indicating the absence of significant populations of conformers with interspin-distances smaller than about 2 nm. Importantly, these measurements ascertained that double mutants did not preferentially stack upon themselves during filament growth. As a consequence, the spin−spin interactions detected by DEER for the diluted filaments must be the result of intramolecular interactions.

DEER measurements were carried out at Q-band (34 GHz) resulting in an ~10-fold increase in sensitivity relative to conventional X-band (9.4 GHz) measurements.[28,37,38] The dipolar oscillation traces for each double mutant are compared for filaments prepared by the three different seeding schemes. The traces for 311/322 indicate similar spin−spin interaction for all three types of filaments (Figure 1a). Markedly, the traces for K19-seeded filaments of K19 and K18 nearly superimpose suggesting similar filament conformations when grown onto the same K19 seeds. This notion is further supported by the oscillation traces of the 311/326 and 311/328 filaments (Figure 1b,c). While the K18-seeded filaments show strong spin−spin interactions (indicated by the rapid initial drop in intensity), the K19-seeded filaments show only weak spin−spin interactions (indicated by the small initial drop in intensity). For both 311/326 and 311/328 the dipolar oscillations for K18 on K19 are similar to those for K19 and dramatically different than for K18. In fact, doubly labeled K19 filaments produce an oscillation trace that is similar to that for singly labeled K19 controls (compare green and red traces in Figure 1b) implying interspin distances above 5 nm. These longer distance conformers are also dominant in the K19-seeded K18 filaments for 311/326 and 311/328. However, the slightly greater drop in the initial intensities (compare the blue with red traces)

dx.doi.org/10.1021/ja303498q | J. Am. Chem. Soc. 2012, 134, 10271−10278

suggests the existence of a minor subpopulation of K18 filaments with smaller interspin distances.

In summary, our experiments reveal major structural differences between K18 and K19 seeded filaments and provide molecular evidence for the conformational plasticity of K18, which assumes the conformations of its seeds.

Tau Filaments Are Heterogeneous. To determine the interspin distances for the differently labeled K18 filaments, the dipolar oscillation traces in Figure 1 were fit by Tikhonov regularization[39] in the time and frequency domains (Figure 2a,b). The resulting distance distributions (Figure 2c) revealed

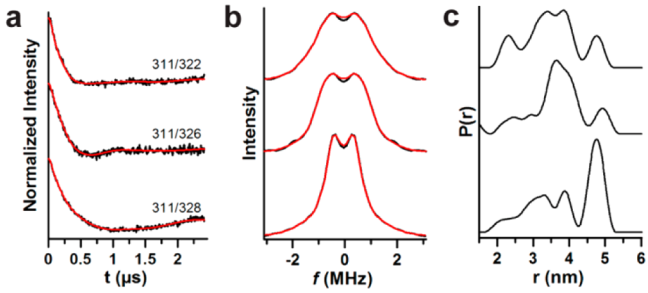

Figure 2. Analysis of DEER data for K18 311/322, 311/326, and 311/328 grown onto K18 seeds reveals structurally heterogeneous filaments. Fitting by Tikhonov regularization is shown in red on the dipolar evolution curves after background subtraction in (a) time domain and (b) frequency domain. (c) Distance distributions. The broad distributions indicate coexistence of multiple conformers of K18 filaments.

major peaks at 3.2 and 3.8 nm for 311/322, 3.5 and 4.0 nm for 311/326, and 4.8 nm for 311/328. Additional peaks with smaller amplitudes are observed for all three double mutants. Analysis of dipolar oscillation curves recorded with different numbers of scans, and therefore differing signal-to-noise, gave consistent distance distributions. The distance distributions shown in Figures 2 and 3 were obtained by using a homogeneous three-dimensional function for the background subtraction because it gave the best fit to the curves for filaments obtained from singly labeled tau. The results indicate that the distributions of interspin distances are due to heterogeneity of the filament conformation and conformations

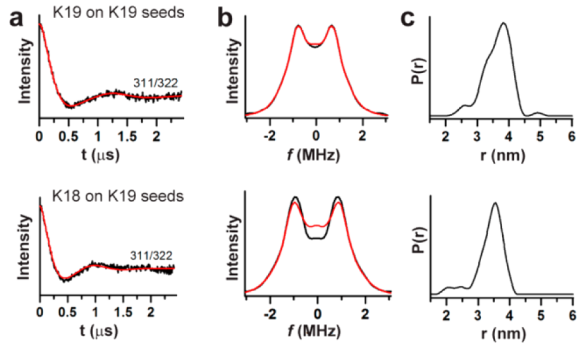

Figure 3. Tau filaments seeded with K19 are structurally homogeneous. DEER data are analyzed by Tikhonov regularization. K19 311/322 grown on K19 seeds (upper row). K18 311/322 grown on K19 seeds (lower row). Best fits in red on background corrected evolution curves in (a) time domain and (b) frequency domain. (c) Distance distributions. The narrow distributions indicate a limited number of conformers.

of the spin label, rather than errors introduced by Tikhonov regularization.

The oscillation traces for filaments of K19 or K18 grown on K19 were fit in an analogous manner (Figure 3a,b). The 311/322 mutants provided meaningful distance distributions (Figure 3c). Notably, the distance distributions for 311/322 were comparable for K19 and K18 grown on K19 (major interspin distance of 3.5−3.7 nm), supporting the model of similar filament conformations. For 311/326 and 311/328, the dipolar oscillation traces for K19 or K18 grown on K19 were quite similar to those for singly labeled mutants, which indicates that the dominant conformers have long interspin distances (above) that are not accessible to DEER distance determination with the 2.4 μs data acquisition windows. The length of the data acquisition window was limited by the short spin echo dephasing time, T_m, of ∼1.2−1.4 μs for these samples.

Structural Insights into the Heterogeneous Folding of Tau Filaments. Previous work has suggested that each tau repeat is a folding unit within the filament[3,40,41] and that R3 could be categorized into at least three different types of conformations: (1) straight-line (SL)-shape, (2) L-shape, and (3) U-shape (Figure 4).[41] Here, we asked whether these modeled conformations could help in the interpretation of the experimentally derived distance distributions.

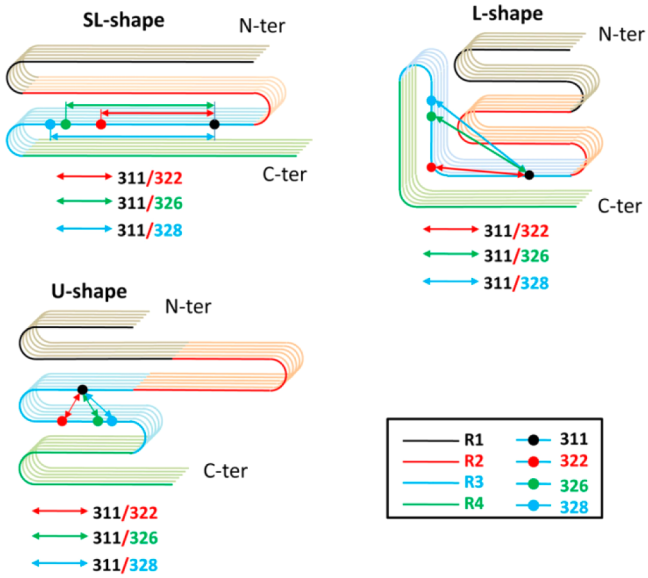

Figure 4. Structural models of tau filaments. The K18 models were optimized by extensive molecular dynamics simulations and emphasize the three basic conformations of the third repeat (blue): SL-, L-, and U-shapes, which have also been modeled for K19 filaments.[41] The remaining tau repeats are represented by different colors. These repeats can assume additional conformations.[41] However, for clarity, those conformations are not depicted. Labeled residues (Cα) are indicated by colored dots. Pairs of labels for which distances were determined by DEER are labeled by arrows. Repeats 1−4 are abbreviated as R1−R4.

Based on extensive molecular dynamics simulations of wild-type K18 and K19 with explicit water solvation, the calculated distances between the nonhydrogen terminal atoms for the native side chains of K18 and K19 for 311/322, 311/326, and 311/328 in the SL-conformation are shown in Figure S4, Supporting Information. The relatively narrow distance distributions indicated that the modeled side chains are in

dx.doi.org/10.1021/ja303498q | J. Am. Chem. Soc. 2012, 134, 10271−10278

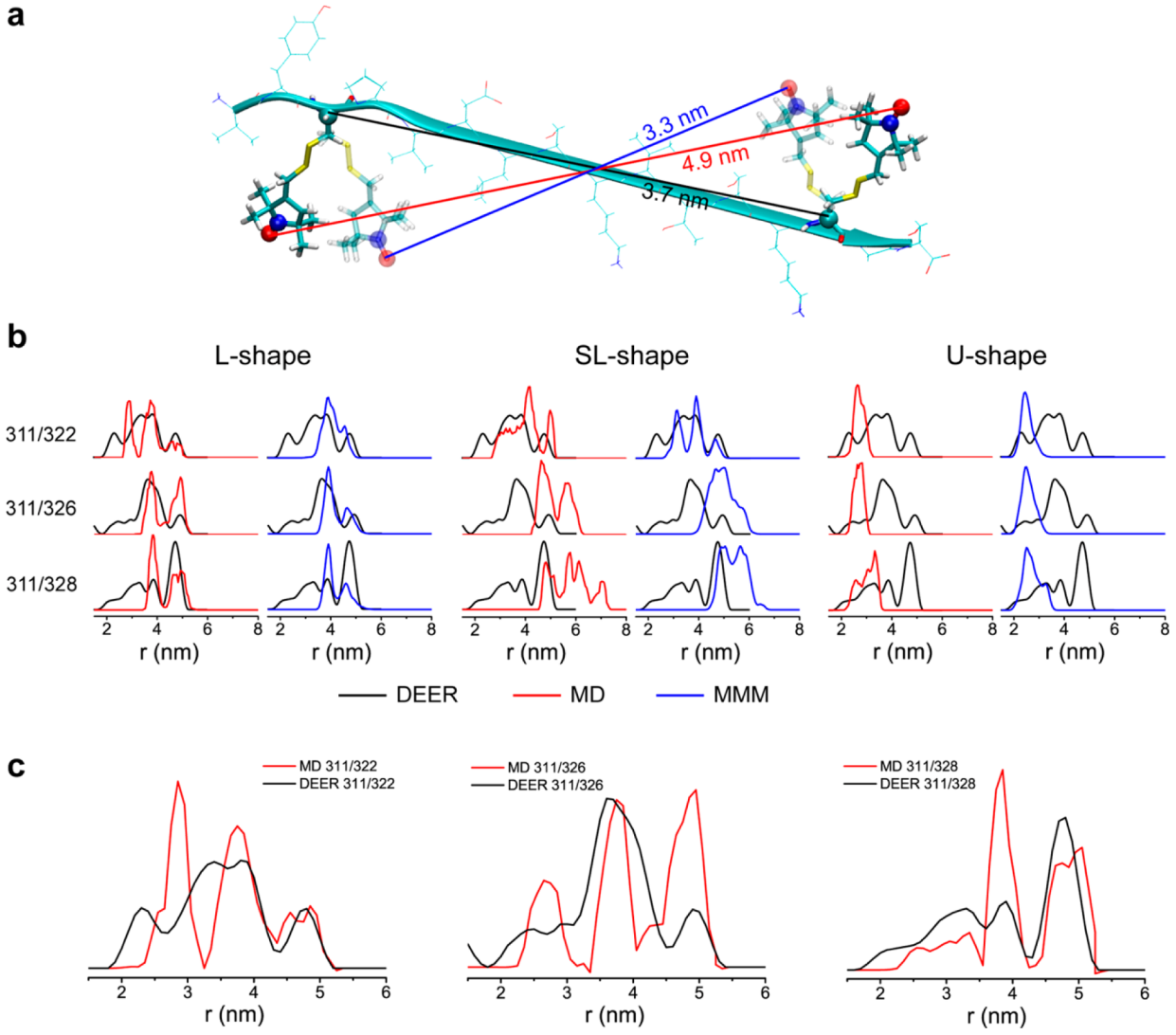

Figure 5. K18 filaments are composed of at least three distinct conformers. (a) Different rotamer arrangements within the tau filament, exemplified by MD snapshots from the labeled 311/322 pair in SL-shape, contribute to the measured distance distribution in K18. The nitroxyl groups are represented as spheres (blue: N atom, red: O atom). (b) Experimental DEER data are overlaid with simulated distance distributions for the three basic conformers of R3: L-, SL-, and U-shapes (see Figure 4). DEER observations are represented in black, MD results in red, and MMM results in blue. A mixture of different filament conformers explains the DEER distance distributions. (c) Comparisons of experimental distance distributions and simulated distributions of the mixture of three conformers (L:SL:U = 6:3:1) for 311/322 (left), 311/326 (center), and 311/328 (right). Same color coding as in (b). The global fitting reveals a minimum of 30% SL-shape structure in K18 filaments.

compact environments with limited side chain rotamer distributions. Therefore it was assumed that although the nitroxyl side chains attached to mutated cysteines are larger than the native side chains, the orientations of the spin labels would be similar to the orientations of the native side chains. For the SL-conformations, the inter-side chain distances for 311/326 and 311/328 are much longer than for 311/322. These predictions are in qualitative agreement with the DEER results for K19 and K18 on K19, where the conformations for 311/326 and 311/328 have nitroxyl−nitroxyl distances that are too long for characterization by DEER of tau samples with short phase memory times. Quantitative distance comparisons require explicit inclusion of the labels.

The observations that nitroxyl−nitroxyl distances for K18 311/322, 311/326, and 311/328 are within the range detectable by DEER indicate that conformations are different than for K19, and conformations other than SL need to be considered. For nitroxyl spin labels the unpaired spin density is localized predominantly on the >NO moiety, so distances obtained by DEER are the >NO to >NO distances which are approximated as oxygen−oxygen distances. To identify which R3 conformer has the highest population in the K18 filaments, we simulated the distributions of the distances between the two nitroxyl groups in spin-labeled molecules based on the aforementioned three models. First, three pentamers of each model were used to represent the filament structure. For each pentamer, double Cys mutations were made in the middle chain at 311/322, 311/326, and 311/328, respectively, as in the DEER experiments. The rotamer distributions of the labeled side chain (Figure 5a) were calculated by a combined molecular dynamics simulation and Monte Carlo method (MD-MC) and Gunnar Jeschke's MMM algorithm.[42] In the MMM algorithm conformations of the spin label that fit into the local peptide structure are selected from a library of conformations observed in X-ray crystal structures of spin-labeled proteins. As shown in Figure 5b and Table S1, Supporting Information, the results

dx.doi.org/10.1021/ja303498q | J. Am. Chem. Soc. 2012, 134, 10271−10278

calculated by the MD-MC and the MMM methods are similar. The MD-MC distributions are in better agreement with the observed DEER spectra and reveal finer details for L-shape. The distributions in the U-shape model indicate shorter distances than the DEER observation, which suggests that the U-shape model is not the major populated structure in K18 filaments. The major peaks in the 311/322 mutant in the L- and SL-shapes do not show large differences, since in both L- and SL-shape models, the residues at positions 311−322 protrude from an almost straight line (Figure 4). However, because the environments of the L- and SL-shape models differ, the minor peaks show some significant differences. The major peaks in the 311/326 and 311/328 mutants present large differences between the L- and SL-shapes. The MD-MC calculations of the distance distributions for the L-shaped 311/326 and 311/328 mutants almost overlap the DEER observation for the K18 filament, while the SL-shape distributions present distances that are slightly longer than 5.0 nm. The comparison of experimental and calculated results suggests that K18 filaments are heterogeneous with contributions from different conformers. K19 and K18 filaments grown on K19 seeds by contrast are more homogeneous and dominated by SL-shape conformations.

We then analyzed the possible population distribution of the three filament structures in the K18 filaments by fitting DEER observation with a mixture of the three structural models (L-, SL-, and U-shapes). The MD-MC method is more suitable for population distribution calculation since it can be weighted using Boltzmann energy distribution, while the MMM method can only use a simple average value from three conformers. As shown in Figure S5, Supporting Information, the 311/328 mutant can be well fitted with the ratio of L:SL:U = 1:6:1, indicating that the highest percentage of SL-shape structure could be 75%. However, at this high SL-shape ratio, the fittings of the 311/322 and 311/326 mutants are less satisfactory (Figure S5, Supporting Information), indicating that the spin-labeled double mutants have varied preferences for different conformers. The global fitting for the three mutants: 311/322, 311/326, and 311/328 can be obtained by a mixture of L:SL:U = 6:3:1 (Figure 5c), suggesting at least 30% SL-shape structure. Thus, our study indicates that the population of SL-shape structure in heterogeneous K18 filaments could be in the range of 30−75%. It should be noted that the structural models are derived computationally and hence may not comprise the full spectrum of possible structures. This could explain the reduced number of rotamers that is observed for K19 seeded filaments (Figure 3c) and the absence of any modulation in the 311/326 and 311/328 filaments of K19 (Figure 1b,c). Additional experimental constraints will be necessary to gain further structural insights. Regardless of the specific conformation, the population analysis offers a possible explanation why homogeneous K19 filaments can seed K18 monomers, but heterogeneous K18 filaments fail to recruit K19 monomers. The overall height of the latter barrier might be further modulated by sequence and conformation incompatibilities between the two different tau isoforms.

DISCUSSION

Tau filaments are characterized by an asymmetric barrier in which monomers of 4R tau can grow onto filaments of 3R tau; however, monomers of 3R tau cannot grow onto filaments of 4R tau.[25] Here we have used site-directed spin labeling in conjunction with DEER spectroscopy to elucidate the molecular basis for this cross-seeding barrier. A set of three doubly labeled cysteine mutants (311/322, 311/326, and 311/328) reveals large-scale conformational variations in the third repeat of K18 (4R) and K19 (3R). Specifically, the distances between spin labels in K19 filaments indicate a fully extended conformation, while the distances in K18 filaments are suggestive of bends. Importantly, when K18 monomers are cross-seeded with K19 filaments, the newly incorporated monomers assume the extended conformation of the seeds. This conformation is stable over multiple cycles of seeding and amplification, as K18 filaments retain their ability to effectively recruit K19 monomers.[25] The distance measurements provide compelling molecular evidence for the structural plasticity of tau[43] as the initial seeds imprint their conformation onto the recruited K18 monomers. The measurements further indicate that when aggregated by themselves, K18 monomers form a heterogeneous mixture of filaments with dominant subspecies. Computational simulations suggest that the ratio of the bent conformer to the fully extended conformation could be around 2:1.

Structural heterogeneity, conformation-based seeding barriers, and emergence of new fibril strains are important characteristics of prions and are thought to be intimately associated with function. Here we show that similar structural characteristics also hold for tau. Although there is currently no evidence linking different tau filament conformations to different tauopathies, the recently observed transmission of tau filaments between cells in tissue culture[19] and trans-synaptic spreading of tau pathology in vivo[44,45] suggests that such connections may exist. Insights gained from prions might serve as viable mechanistic models for tau.

A serious challenge to the protein-only hypothesis of prion transmission was the question of how a single protein could account for different strains or variants. Multiple lines of evidence from mammalian prions have shown that distinct conformers could encode the information for these differences.[46−48] Similar conclusions were derived from the experimentally more tractable yeast prions (which show no sequence homology to their mammalian counterparts). The transformation of conformationally distinct fibrils of Sup35p[49,50] and Ure2p[51] into yeast cells resulted in distinct phenotypes that could be propagated over multiple generations. Conformational diversity of protein fibrils has also been observed for other amyloids, such as Aβ[52] and α-synuclein,[53] although as with tau, a clear link to different disease phenotypes has not yet been established.

It has long been recognized that variations in amino acid sequence between prion proteins are associated with barriers in transmission.[54] The substitution of only one or two amino acids can result in a robust barrier if positioned in a key region of the protein.[55,56] Since a particular sequence can result in a spectrum of different fibril conformers,[17,18] each conformer will have its own seeding characteristics. As a consequence, the seeding barrier will be determined not only by sequence but also by conformation and conformation population distributions.[17,18] Changes in the cellular environment could affect the composition of fibril conformers[57] and hence influence the seeding barrier. It is interesting to note that in a cell-free system, seeds of the P301L mutant of tau prevented growth of wild-type tau,[58] while in cell culture this barrier did not exist.[22] Similarly, seeds of 3R tau incorporated 4R tau in vitro, yet in cell culture no such incorporation was observed.[59] In contrast, the barrier which prevents growth of 3R tau onto 4R tau seeds

exists under both in vitro and in vivo conditions, suggesting that 3R tau is compatible with only a very small number of 4R tau conformers. One such conformer emerges through the cross-seeding of 4R tau with 3R tau seeds.[25]

The emergence of new strains after the crossing of a transmission barrier is a well-known property of prions. For example, variant Creutzfeldt Jacob disease has been linked to the transmission of bovine prions to humans.[60] In this process, the human prion protein is thought to assume the conformation of the bovine template. Convincing molecular evidence for the emergence of new prion strains has been presented using the prion protein variant Y145Stop.[61] A mouse prion variant that was seeded with hamster prion fibrils resulted in a new fibril type that had the capacity to seed hamster prions. Importantly, when mouse prion fibrils were formed in the absence of hamster prion seeds, a barrier existed between the different proteins. The asymmetric barrier that is observed for filaments of 3R and 4R tau and the emergence of a new 4R tau conformer upon seeding with 3R tau resembles these prion characteristics.

The underlying basis for these overall similarities must reside within the shared structural properties of the amyloid fold and conformational selections among the different structures. Amyloid fibrils together with other cellular components provide a non-DNA-based means for propagating information.[62] It is tempting to speculate that the phenotypic diversity of human tauopathies could be linked to different conformers and that preferential deposition of 3R tau in Pick's disease and 4R tau in progressive supranuclear palsy could be based on differential seeding properties and clearance of slowly propagating strains. If tau filaments are ensembles of conformers, the question arises whether the composition of these ensembles could change as the aggregates transferred between different neurons. The recently observed evolution of prions in cell culture[63] suggests that such diversification is possible. With the ability to resolve different conformers within a heterogeneous mixture, the herein presented DEER approach, in combination with large scale molecular dynamics simulations, provides a new powerful tool to investigate the composition and dynamics of amyloid ensembles.

■ ASSOCIATED CONTENT

Supporting Information

Additional experimental procedures, Figures S1−S5, and Table S1. This material is available free of charge via the Internet at http://pubs.acs.org.

■ AUTHOR INFORMATION

Corresponding Author

martin.margittai@du.edu

Notes

The authors declare no competing financial interest.

■ ACKNOWLEDGMENTS

This project was supported by National Institute of Neurological Disorders and Stroke Grant R01NS076619 (to M.M.). This work was also supported by National Cancer Institute contract HHSN261200800001E, the intramural research program of the National Cancer Institute Center for Cancer Research, National Science Foundation CAREER Award CBET-0952624 (to J.Z.), a 3M nontenured faculty award (to J.Z.), National Natural Science Foundation of China Grant 11074047 (to G.W.), and Research Fund for the Doctoral Program of Higher Education of China Grant RFDP-20100071110006 (to G.W.).

■ REFERENCES

(1) Goedert, M.; Spillantini, M. G. *J. Mol. Neurosci.* **2011**, *45*, 425−31.
(2) Lee, V. M.; Goedert, M.; Trojanowski, J. Q. *Annu. Rev. Neurosci.* **2001**, *24*, 1121−59.
(3) Siddiqua, A.; Margittai, M. *J. Biol. Chem.* **2010**, *285*, 37920−6.
(4) Goedert, M.; Spillantini, M. G.; Cairns, N. J.; Crowther, R. A. *Neuron* **1992**, *8*, 159−68.
(5) Buee, L.; Delacourte, A. *Brain Pathol.* **1999**, *9*, 681−93.
(6) Novak, M.; Kabat, J.; Wischik, C. M. *Embo J.* **1993**, *12*, 365−70.
(7) Wischik, C. M.; Novak, M.; Edwards, P. C.; Klug, A.; Tichelaar, W.; Crowther, R. A. *Proc. Natl. Acad. Sci. U.S.A.* **1988**, *85*, 4884−8.
(8) Goedert, M.; Jakes, R.; Spillantini, M. G.; Hasegawa, M.; Smith, M. J.; Crowther, R. A. *Nature* **1996**, *383*, 550−3.
(9) Barghorn, S.; Mandelkow, E. *Biochemistry* **2002**, *41*, 14885−96.
(10) Friedhoff, P.; von Bergen, M.; Mandelkow, E. M.; Davies, P.; Mandelkow, E. *Proc. Natl. Acad. Sci. U.S.A.* **1998**, *95*, 15712−7.
(11) Jarrett, J. T.; Lansbury, P. T., Jr. *Cell* **1993**, *73*, 1055−8.
(12) von Bergen, M.; Barghorn, S.; Li, L.; Marx, A.; Biernat, J.; Mandelkow, E. M.; Mandelkow, E. *J. Biol. Chem.* **2001**, *276*, 48165−74.
(13) Berriman, J.; Serpell, L. C.; Oberg, K. A.; Fink, A. L.; Goedert, M.; Crowther, R. A. *Proc. Natl. Acad. Sci. U.S.A.* **2003**, *100*, 9034−8.
(14) Sunde, M.; Blake, C. *Adv. Protein Chem.* **1997**, *50*, 123−59.
(15) Wille, H.; Bian, W.; McDonald, M.; Kendall, A.; Colby, D. W.; Bloch, L.; Ollesch, J.; Borovinskiy, A. L.; Cohen, F. E.; Prusiner, S. B.; Stubbs, G. *Proc. Natl. Acad. Sci. U.S.A.* **2009**, *106*, 16990−5.
(16) Eichner, T.; Radford, S. E. *Mol. Cell* **2011**, *43*, 8−18.
(17) Miller, Y.; Ma, B.; Nussinov, R. *Chem. Rev.* **2010**, *110*, 4820−38.
(18) Collinge, J.; Clarke, A. R. *Science* **2007**, *318*, 930−6.
(19) Frost, B.; Jacks, R. L.; Diamond, M. I. *J. Biol. Chem.* **2009**, *284*, 12845−52.
(20) Kfoury, N.; Holmes, B. B.; Jiang, H.; Holtzman, D. M.; Diamond, M. I. *J. Biol. Chem.* **2012**, *287*, 19440−51.
(21) Clavaguera, F.; Bolmont, T.; Crowther, R. A.; Abramowski, D.; Frank, S.; Probst, A.; Fraser, G.; Stalder, A. K.; Beibel, M.; Staufenbiel, M.; Jucker, M.; Goedert, M.; Tolnay, M. *Nat. Cell Biol.* **2009**, *11*, 909−13.
(22) Guo, J. L.; Lee, V. M. *J. Biol. Chem.* **2011**, *286*, 15317−31.
(23) Miller, Y.; Ma, B. Y.; Nussinov, R. *Biochemistry* **2011**, *50*, 5172−5181.
(24) Ma, B.; Nussinov, R. *J. Mol. Biol.* **2011**.
(25) Dinkel, P. D.; Siddiqua, A.; Huynh, H.; Shah, M.; Margittai, M. *Biochemistry* **2011**, *50*, 4330−6.
(26) Milov, A. D.; Salikhov, K. M.; Shchirov, M. D. *Sov. Phys. Solid State* **1981**, *23*, 565−569.
(27) Jeschke, G.; Pannier, M.; Spiess, H. W. *Biol. Magn. Reson.* **2000**, *19*, 493−512.
(28) Swanson, M. A.; Kathirvelu, V.; Majtan, T.; Frerman, F. E.; Eaton, G. R.; Eaton, S. S. *Protein Sci.* **2011**, *20*, 610−20.
(29) Fajer, P. G.; Brown, L.; Song, L. *Biol. Magn. Reson.* **2007**, *27*, 95−128.
(30) Jeschke, G.; Chechnik, V.; Ionita, P.; Godt, A.; Zimmermann, H.; Banham, J.; Timmel, C. R.; Hilger, D.; Jung, H. *Appl. Magn. Reson.* **2006**, *30*, 473−498.
(31) Kale, L.; Skeel, R.; Bhandarkar, M.; Brunner, R.; Gursoy, A.; Krawetz, N.; Phillips, J.; Shinozaki, A.; Varadarajan, K.; Schulten, K. *J. Comput. Phys.* **1999**, *151*, 283−312.
(32) Zheng, J.; Ma, B. Y.; Chang, Y.; Nussinov, R. *Front. Biosci.* **2008**, *13*, 3919−3930.
(33) Bedrood, S.; Li, Y.; Isas, J. M.; Hegde, B. G.; Baxa, U.; Haworth, I. S.; Langen, R. *J. Biol. Chem.* **2012**, *287*, 5235−41.
(34) Karyagina, I.; Becker, S.; Giller, K.; Riedel, D.; Jovin, T. M.; Griesinger, C.; Bennati, M. *Biophys. J.* **2011**, *101*, L1−3.

(35) Margittai, M.; Langen, R. *Proc. Natl. Acad. Sci. U.S.A.* **2004**, *101*, 10278−83.
(36) Margittai, M.; Langen, R. *Q. Rev. Biophys.* **2008**, *41*, 265−97.
(37) Ghimire, H.; McCarrick, R. M.; Budil, D. E.; Lorigan, G. A. *Biochemistry* **2009**, *48*, 5782−4.
(38) Zou, P.; Mchaourab, H. S. *Biophys. J.* **2010**, *98*, L18−20.
(39) Chiang, Y. W.; Borbat, P. P.; Freed, J. H. *J. Magn. Reson.* **2005**, *172*, 279−295.
(40) Margittai, M.; Langen, R. *J. Biol. Chem.* **2006**, *281*, 37820−7.
(41) Yu, X.; Luo, Y.; Dinkel, P.; Zheng, J.; Wei, G.; Margittai, M.; Nussinov, R.; Ma, B. *J. Biol. Chem.* **2012**, *287*, 14950−14959.
(42) Polyhach, Y.; Bordignon, E.; Jeschke, G. *Phys. Chem. Chem. Phys.* **2011**, *13*, 2356−2366.
(43) Frost, B.; Ollesch, J.; Wille, H.; Diamond, M. I. *J. Biol. Chem.* **2009**, *284*, 3546−51.
(44) Liu, L.; Drouet, V.; Wu, J. W.; Witter, M. P.; Small, S. A.; Clelland, C.; Duff, K. *PLoS One* **2012**, *7*, e31302.
(45) de Calignon, A.; Polydoro, M.; Suarez-Calvet, M.; William, C.; Adamowicz, D. H.; Kopeikina, K. J.; Pitstick, R.; Sahara, N.; Ashe, K. H.; Carlson, G. A.; Spires-Jones, T. L.; Hyman, B. T. *Neuron* **2012**, *73*, 685−97.
(46) Bessen, R. A.; Marsh, R. F. *J. Virol.* **1994**, *68*, 7859−68.
(47) Telling, G. C.; Parchi, P.; DeArmond, S. J.; Cortelli, P.; Montagna, P.; Gabizon, R.; Mastrianni, J.; Lugaresi, E.; Gambetti, P.; Prusiner, S. B. *Science* **1996**, *274*, 2079−82.
(48) Peretz, D.; Scott, M. R.; Groth, D.; Williamson, R. A.; Burton, D. R.; Cohen, F. E.; Prusiner, S. B. *Protein Sci.* **2001**, *10*, 854−63.
(49) Tanaka, M.; Chien, P.; Naber, N.; Cooke, R.; Weissman, J. S. *Nature* **2004**, *428*, 323−8.
(50) King, C. Y.; Diaz-Avalos, R. *Nature* **2004**, *428*, 319−23.
(51) Brachmann, A.; Baxa, U.; Wickner, R. B. *Embo J.* **2005**, *24*, 3082−92.
(52) Petkova, A. T.; Leapman, R. D.; Guo, Z.; Yau, W. M.; Mattson, M. P.; Tycko, R. *Science* **2005**, *307*, 262−5.
(53) Heise, H.; Hoyer, W.; Becker, S.; Andronesi, O. C.; Riedel, D.; Baldus, M. *Proc. Natl. Acad. Sci. U.S.A.* **2005**, *102*, 15871−6.
(54) Prusiner, S. B.; Scott, M.; Foster, D.; Pan, K. M.; Groth, D.; Mirenda, C.; Torchia, M.; Yang, S. L.; Serban, D.; Carlson, G. A.; Hoppe, P. C.; Westaway, D.; DeArmond, S. J. *Cell* **1990**, *63*, 673−86.
(55) Sigurdson, C. J.; Nilsson, K. P.; Hornemann, S.; Manco, G.; Fernandez-Borges, N.; Schwarz, P.; Castilla, J.; Wuthrich, K.; Aguzzi, A. *J. Clin. Invest.* **2010**, *120*, 2590−9.
(56) Jones, E. M.; Surewicz, W. K. *Cell* **2005**, *121*, 63−72.
(57) Weissmann, C.; Li, J.; Mahal, S. P.; Browning, S. *EMBO Rep.* **2011**, *12*, 1109−17.
(58) Aoyagi, H.; Hasegawa, M.; Tamaoka, A. *J. Biol. Chem.* **2007**, *282*, 20309−18.
(59) Nonaka, T.; Watanabe, S. T.; Iwatsubo, T.; Hasegawa, M. *J. Biol. Chem.* **2010**, *285*, 34885−98.
(60) Collinge, J.; Sidle, K. C.; Meads, J.; Ironside, J.; Hill, A. F. *Nature* **1996**, *383*, 685−90.
(61) Vanik, D. L.; Surewicz, K. A.; Surewicz, W. K. *Mol. Cell* **2004**, *14*, 139−45.
(62) Wickner, R. B.; Edskes, H. K.; Ross, E. D.; Pierce, M. M.; Baxa, U.; Brachmann, A.; Shewmaker, F. *Annu. Rev. Genet.* **2004**, *38*, 681−707.
(63) Li, J.; Browning, S.; Mahal, S. P.; Oelschlegel, A. M.; Weissmann, C. *Science* **2010**, *327*, 869−72.